BIOCHEMISTRY
including biophysical chemistry & molecular biology
Article

Biochemistry **2010,** *49,* 8709–8720 8709
DOI: 10.1021/bi100914z

Structures of Cytochrome P450 2B4 Complexed with the Antiplatelet Drugs Ticlopidine and Clopidogrel[†,‡]

Sean C. Gay,[*,§,@] Arthur G. Roberts,[*,§,@] Keiko Maekawa,[∥] Jyothi C. Talakad,[§] Wen-Xu Hong,[⊥] Qinghai Zhang,[⊥] C. David Stout,[⊥] and James R. Halpert[§]

[§]*Skaggs School of Pharmacy and Pharmaceutical Sciences, University of California, San Diego, La Jolla, California 92093,* [∥]*Division of Medicinal Safety Science, National Institute of Health Sciences, Tokyo 158-8501, Japan, and* [⊥]*Department of Molecular Biology, The Scripps Research Institute, La Jolla, California 92037.* [@]*These authors contributed equally to this work.*

Received June 7, 2010; Revised Manuscript Received August 20, 2010

ABSTRACT: Prior X-ray crystal structures of rabbit cytochrome P450 2B4 (2B4) in complexes with various imidazoles have demonstrated markedly different enzyme conformations depending on the size of the inhibitor occupying the active site. In this study, structures of 2B4 were determined with the antiplatelet drugs clopidogrel and ticlopidine, which were expected to have greater freedom of movement in the binding pocket. Ticlopidine could be modeled into the electron density maps in two distinct orientations, both of which are consistent with metabolic data gathered with other mammalian P450 enzymes. Results of ligand docking and heme-induced NMR relaxation of drug protons showed that ticlopidine was preferentially oriented with the chlorophenyl group closest to the heme. Because of its stereocenter, clopidogrel was easier to fit in the electron density and exhibited a single orientation, which points the chlorophenyl ring toward the heme. The C_α traces of both complexes aligned very well with each other and revealed a compact, closed structure that resembles the conformation observed in two previously determined 2B4 structures with the small molecule inhibitors 4-(4-chlorophenyl)imidazole and 1-(4-chlorophenyl)imidazole. The 2B4 active site is able to accommodate small ligands by moving only a small number of side chains, suggesting that ligand reorientation is energetically favored over protein conformational changes for binding of these similarly sized molecules. Adjusting both protein conformation and ligand orientation in the active site gives 2B4 the flexibility to bind to the widest range of molecules, while also being energetically favorable.

Many individual cytochrome P450 forms (P450s) are able to metabolize broad ranges of substrates. Despite sharing a highly conserved fold, different P450s are able to act on molecules of very different sizes and shapes, with remarkable stereo- and regiospecificity. This variability of substrate geometries implies some degree of protein flexibility and adherence to an induced fit model as opposed to the classical lock and key model of one substrate and one enzyme. Over the past decade, a growing list of mammalian P450 crystal structures has confirmed what was already suspected (*1*−*3*), namely that the conformations these enzymes exhibit vary on the basis of the identity of the ligands present.

The largest degree of structural flexibility has been observed in a series of crystal structures of rabbit 2B4 in the presence of various imidazole-based inhibitors (*4*−*7*). When complexed with the small molecules 4-(4-chlorophenyl)imidazole (4-CPI)[1] or 1-(4-chlorophenyl)imidazole (1-CPI), 2B4 adopts a closed structure. This compact conformation has the B−C loop region close to the active site to allow better packing with the small ligands, and the regions between the F and G helices associate with the N-terminus of the protein. The binding of the larger ligands, bifonazole or 1-(4-phenyl)benzylimidazole (1-PBI), results in pivoting of the F−G region over helix I to accommodate the greater inhibitor volumes. The B−C loop also moves in response to the ligands, but in a less predictable fashion. In addition to the B−C and F−G motifs, the 2B4 structures have led to the identification of other plastic regions that are able to reposition secondary structural elements in response to ligand size and shape. However, it was unclear how these structures related to enzyme conformations with pharmaceutically relevant drugs present in the active site. Recent advances in purification and crystallization methods applied to human P450 2B6 (*8*), with which 2B4 shares 78% sequence identity, have helped broaden the spectrum of ligands available for crystallization of 2B4. To explore these new opportunities, we chose to crystallize 2B4 in complex with clopidogrel and ticlopidine, both of which inhibit human 2B6 (*9*).

Clopidogrel and ticlopidine are both thienopyridine, antiplatelet prodrugs (Figure 1), which require activation to their thiol metabolites. The active drugs block binding of ADP to its platelet

[†]This research was supported by National Institutes of Health Grants ES003619 to J.R.H. and GM073197 to Q.Z.

[‡]Atomic coordinates have been deposited at the Protein Data Bank as entries 3KW4 and 3ME6.

*To whom correspondence should be addressed. S.C.G.: e-mail, scgay@ucsd.edu; telephone, (858) 822-7804; fax, (858) 246-0089. A.G.R.: e-mail, a1roberts@ucsd.edu; telephone, (858) 822-7804; fax, (858) 246-0089.

[1]Abbreviations: 4-CPI, 4-(4-chlorophenyl)imidazole; 1-CPI, 1-(4-chlorophenyl)imidazole; 1-PBI, 1-(4-phenyl)benzylimidazole; Cymal-5, 5-cyclohexylpentyl-β-D-maltoside; 232-chol, 3α,7α,12α-tris[(β-D-maltopyranosyl)ethyloxy]cholane; 234-chol, 3α-hydroxy-7α,12α-bis({[2-(trimethylamino)ethyl]phosphoryl}ethyloxy)cholane; BME, 2-mercaptoethanol; PMSF, phenylmethanesulfonyl fluoride; Ni-NTA, nickel-nitrilotriacetic acid; EDTA, ethylenediaminetetraacetic acid; DTT, dithiothreitol; 7-EFC, 7-ethoxy-4-trifluoromethylcoumarin; SSRL, Stanford Synchrotron Radiation Lightsource; PCA, principal component analysis; SVD, singular-value decomposition; rmsd, root-mean-square deviation.

Published on Web 09/03/2010

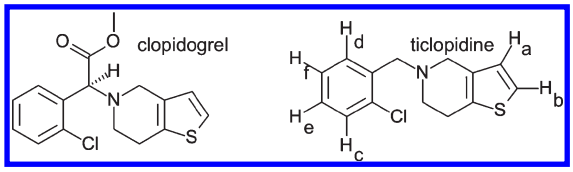

FIGURE 1: Chemical structures of the antiplatelet prodrugs clopidogrel and ticlopidine. The ticlopidine structure includes proton labels used for NMR studies as described in Materials and Methods. BKchem version 0.13.0 (2009, http://bkchem.zirael.org/index.html) was used for drawing chemical structures.

receptor, $P2Y_{12}$, by an irreversible covalent modification of a cysteine residue. This inhibits platelet aggregation and greatly reduces the risk of vascular disease, myocardial infarction, and stroke (*10*). Combined with an aspirin regimen, both drugs have been shown to enhance the prevention of additional ischemic events in high-risk patients (*11*).

P450-mediated oxidation of ticlopidine and clopidogrel leads to numerous products. In vivo studies have identified three primary means of metabolism for ticlopidine in rats and humans resulting from N-dealkylation, N-oxidation, and oxidation of the thiophene ring (*12*, *13*). However, in vitro studies have found additional ticlopidine metabolites, including a thiophene *S*-oxide dimer formed by 2C19 and 2D6 (*14*), dihydrothienopyridinium and thienopyridinium species formed by 1A2, 2C9, 2C19, 2D6, and 3A4 (*15*), and two hydroxyl metabolites formed in rat liver microsomes that occur via epoxidation of the chlorophenyl ring (*16*). Additionally, oxidation of the thiophene ring of clopidogrel to various compounds has been shown to be catalyzed by 1A2, 2B6, 2C9, 2C19, and 3A4 (*17*). Presumably, the products that are formed are related to the orientation the drug adopts in the active site.

Metabolites formed via oxidation of the thiophene ring are known to inhibit several P450s, including 1A2, 2B6, 2C9, 2C19, and 2D6 (*9*, *18*). It has been shown that during metabolism of ticlopidine, the formation of either a thiolactone or thiophene *S*-oxide intermediate results in mechanism-based inactivation of 2C19 and possibly 2D6 (*14*). Because 2B6 also produces a thiolactone intermediate during clopidogrel metabolism (*17*) and is inactivated by both clopidogrel and ticlopidine (*9*), it has been inferred that the 2B6 inactivation process occurs by a mechanism similar to that of 2C19. The inhibition of P450s is known to create adverse drug−drug interactions, which could lead to increased toxicity of pharmaceuticals during combined therapeutic regimens. However, P450 mechanism-based inactivation results in more severe effects because cells must synthesize new proteins to replace those that have been inactivated (*19*). It has been reported that bupropion hydroxylation by 2B6 was suppressed by clopidogrel and ticlopidine by 68 and 90%, respectively (*20*). Also, 2C19 activity toward both phenytoin and omeprazole is inhibited by ticlopidine (*21*, *22*). These results indicate that the antiplatelet drugs clopidogrel and ticlopidine may significantly alter the metabolism of other drugs that are metabolized by these P450s and possibly others.

Given the sequence and structural similarities between 2B6 and 2B4 (*8*), the greater number of 2B4 crystal structures for comparison and analysis (*4*−*7*, *23*), and the wealth of biochemical data gathered for 2B4 (*3*, *24*), this enzyme was selected for crystallization with both drugs. This study describes the structures of the clopidogrel and ticlopidine complexes of 2B4 determined by X-ray crystallography. To investigate the preferred orientation of ticlopidine deduced from X-ray crystallography in the active site, heme-induced NMR relaxation of ligand protons (*25*−*27*) by 2B4 was used. Ligand docking of ticlopidine in the active site also supported the NMR results. The two crystal structures reported here are the first examples of 2B4 bound to non-imidazole-based inhibitors.

MATERIALS AND METHODS

Materials. Ribonuclease A, ticlopidine, and clopidogrel were from Sigma-Aldrich (St. Louis, MO). 5-Cyclohexylpentyl-β-D-maltoside (Cymal-5) was from Anatrace (Maumee, OH). The 50 kDa molecular mass protein cutoff Amicon Ultra filtration devices were from Millipore (Billerica, MA). Nickel-nitrilotriacetic acid affinity resin was from Qiagen (Valencia, CA). DE52 anion exchange resin was from Whatman (Maidstone, Kent, U.K.). Macroprep CM cation exchange resin was from Bio-Rad Laboratories (Hercules, CA). TOPP3 cells were from Stratagene (La Jolla, CA). Wizard I and Wizard II crystallization screens were from Emerald Biosystems (Bainbridge Island, WA). The synthesis of the facial amphiphiles 3α,7α,12α-tris[(β-D-maltopyranosyl)ethyloxy]cholane (232-chol) and 3α-hydroxy-7α,12α-bis({[2-(trimethylamino)ethyl]phosphoryl}ethyloxy)cholane (234-chol) was performed essentially according to a previous method (*28*) and will be reported in more detail elsewhere. Human cytochrome P450 2B6dH (2B6) was expressed and purified as described previously (*8*).

Protein Expression and Purification. Cytochrome P450 2B4dH(H226Y) (2B4) was expressed in *Escherichia coli* TOPP3 cells as described previously (*4*). The H226Y mutant is used to avoid the dimerization seen in the ligand-free structure (*23*). Protein purification was conducted according to the method of Gay et al. (*8*). Briefly, an overnight, Luria-Bertani broth culture of *E. coli* containing the pKK2B4dH(H226Y) plasmid was used to inoculate Terrific broth. Terrific broth cultures were grown at 37 °C until A_{600} reached approximately 1.0. Protein expression was induced by the addition of isopropyl β-D-1-thiogalactopyranoside and δ-aminolevulinic acid. Protein expression continued for 60−69 h at 30 °C, after which the cells were harvested by centrifugation. The cell pellet was resuspended in 10% of the original culture volume in buffer containing 20 mM potassium phosphate (pH 7.4 at 4 °C), 20% (v/v) glycerol, 10 mM 2-mercaptoethanol (BME), and 1.0 mM phenylmethanesulfonyl fluoride (PMSF). The resuspended cells were further treated with lysozyme (0.3 mg/mL) and stirred for 30 min at 4 °C, followed by a brief centrifugation for 15 min at 7000 rpm in a JA-14 rotor in an Avanti J-26 XPI Centrifuge (Beckman Coulter, Inc., Fullerton, CA). Spheroplasts were again resuspended in 5% of the original culture volume in buffer containing 500 mM potassium phosphate (pH 7.4 at 4 °C), 20% (v/v) glycerol, 10 mM BME, and 0.5 mM PMSF and were sonicated three times for 45 s on ice. The membrane pellet was separated by centrifugation for 10 min at 7000 rpm in the same centrifuge and rotor described above. Cymal-5 and ribonuclease A were added to the supernatant at final concentrations of 4.8 mM and 4.0 μg/mL, respectively, and this mixture was allowed to stir for 2 h at 4 °C prior to ultracentrifugation for 45 min at 45000 rpm using a fixed-angle Ti 50.2 rotor in an Optima L-80 XP Ultracentrifuge (Beckman Coulter, Inc.). The P450 concentration in the supernatant was determined from reduced CO difference spectra.

The supernatant was loaded onto a prepacked Ni-NTA column and was washed with buffer containing 100 mM potassium phosphate (pH 7.4 at 4 °C), 100 mM NaCl, 20% (v/v) glycerol,

10 mM BME, 0.5 mM PMSF, 4.8 mM Cymal-5, and 1 mM histidine. The protein was eluted using 30 mM histidine in the same buffer described above. The pooled P450-containing fractions were incubated with DE52 resin for 15 min to remove *E. coli* RNA in the sample. The supernatant was collected by centrifugation and diluted 10-fold in buffer containing 5 mM potassium phosphate (pH 7.4 at 4 °C), 20% (v/v) glycerol, 1 mM ethylenediaminetetraacetic acid (EDTA), 0.2 mM dithiothreitol (DTT), 0.5 mM PMSF, and 4.8 mM Cymal-5, prior to being loaded onto a Macroprep CM cation exchange column. The column was washed using 5 mM potassium phosphate (pH 7.4 at 4 °C), 20 mM NaCl, 20% (v/v) glycerol, 1 mM EDTA, and 0.2 mM DTT, and the protein was eluted with high-salt buffer containing 50 mM potassium phosphate (pH 7.4 at 4 °C), 500 mM NaCl, 20% (v/v) glycerol, 1 mM EDTA, and 0.2 mM DTT. Protein fractions with the highest A_{417}/A_{280} ratios were pooled, and the P450 concentration was measured using reduced CO difference spectra.

Spectral Binding. For binding studies, difference spectra were recorded using 1 μM P450 on a 2401 PC spectrophotometer (Shimadzu Corp., Kyoto, Japan) at 25 °C as described previously (*29*). In brief, the difference in absorbance between the maxima and minima (ΔA) was recorded after the addition of a series of ticlopidine and clopidogrel concentrations in methanol to the sample cuvette and the same amount of methanol to the reference cuvette. For the comparison of 2B4 and 2B6, protein samples were maintained in buffer containing 50 mM potassium phosphate (pH 7.4), 500 mM NaCl, 500 mM sucrose, 1 mM EDTA, and 0.2 mM DTT. For the determination of the dissociation constant of ticlopidine under NMR conditions, 2B4 was in 25 mM potassium phosphate (pH 7.0). In both cases, the spectral dissociation constants (K_s) were obtained by fitting the data to the equation for "tight binding" $2\Delta A = (\Delta A_{max}/[E_0])$-$[K_D + [I_0] + [E_0] + (K_D + [I_0] + [E_0])^2 - (4[E_0][I_0])^{1/2}]$, where $[E_0]$ and $[I_0]$ are total enzyme and total inhibitor concentrations, respectively. All data treatment and fitting of the titration curves were performed with our SpectraLab software (*30*) or using Igor Pro version 6.1 (Wavemetrics, Inc., Lake Oswego, OR). In addition to fitting the titrations, the absolute absorbance spectrum of 2B4 with saturating 1.15 mM ticlopidine was fit by a least-squares method using software written in the Python programming language as described previously (*31*).

Enzyme Inhibition. The K_i values were determined using 7-ethoxy-4-trifluoromethylcoumarin (7-EFC) O-deethylation measured in a final reaction volume of 100 μL at drug concentrations of 0.5−5.0 μM and substrate concentrations of 0−150 μM. In brief, the reaction mixture contained 7-EFC in the standard reconstitution system (1:4:2 P450/cytochrome P450 NADPH reductase/cytochrome b_5 mixture) at 10 pmol of P450 in 50 mM HEPES (pH 7.4), 15 mM $MgCl_2$, and 2% methanol. The reaction was performed at 37 °C for 5 min using 1 mM NADPH. The K_i was determined using an enzyme kinetic fit from SigmaPlot (Systat Software, Inc., Point Richmond, CA).

Crystallization and Data Collection. Pooled protein was diluted to 18 μM in 50 mM potassium phosphate (pH 7.4 at 4 °C), 500 mM NaCl, 500 mM sucrose, 1 mM EDTA, and 0.2 mM DTT. Ticlopidine was added to this sample at 54 μM, and the solution was incubated at 4 °C overnight. An additional 30 mL of the buffer described above containing 54 μM ticlopidine was prepared to further dilute the glycerol present in the protein sample. Buffer exchange was performed by concentration of the diluted protein solution to approximately 0.55 mM followed by dilution to 18 μM, and the process was repeated twice before finally concentrating the 2B4−ticlopidine complex to 0.55 mM. The concentrated complex was supplemented with 4.8 mM Cymal-5, 1.65 mM ticlopidine, and 0.028% (w/v) 232-chol. Crystal screening was performed by sitting drop vapor diffusion using the Wizard II high-throughput kit by mixing equal volumes of the 2B4−ticlopidine complex and the well solution. Drops were equilibrated against the well solutions at 18 °C. Crystals for X-ray diffraction grew over the course of 1 week in drops containing a well solution consisting of 20% (w/v) PEG 8000, 0.2 M $MgCl_2$, and 0.1 M Tris (pH 8.5). Crystals were transferred to a solution of mother liquor supplemented with 335 mM sucrose for 3.5 min before being flash-frozen in liquid nitrogen; 120° of data was collected using 0.5° oscillations and 30 s exposures at 100 K on a Quantum CCD detector (Area Detector Systems Corp., Poway, CA) at beamline 11-1 of the Stanford Synchrotron Radiation Lightsource (SSRL) (Stanford, CA). The data were processed to 2.67 Å using iMOSFLM (*32*) and SCALA (*33*).

Clopidogrel was added to pooled 2B4 fractions, which were concentrated as described above, except 0.077% (w/v) 234-chol was substituted for 232-chol. Conditions were screened as described above using the Wizard I high-throughput kit. Crystals grew at 18 °C in drops containing a well solution consisting of 20% (w/v) PEG 8000, 0.2 M NaCl, and 0.1 M phosphate-citrate (pH 4.2). Crystals were transferred to a solution of mother liquor supplemented with 335 mM sucrose for 2 min before being flash-frozen in liquid nitrogen; 155° of data was collected using 0.5° oscillations and 20 s exposures at 100 K on the same detector as described above at beamline 11-1 of SSRL. Because of crystal decay from the X-ray beam, only the first 240 frames (120°) were used and processed to 3.10 Å using iMOSFLM and SCALA.

Structure Determination and Refinement. The 2B4−ticlopidine complex structure was determined by molecular replacement using the previously determined 2B4−4-CPI complex structure [Protein Data Bank (PDB) entry 1SUO] (with the 4-CPI inhibitor removed from the coordinates) in Phaser (*34*). The structure solution determined the space group to be $P3_221$, containing 61.6% solvent assuming one protein molecule per asymmetric unit. The initial model was subjected to rigid body refinement and a restrained refinement using REFMAC (*35*). Model building was performed in COOT (*36*) using both $2F_o - F_c$ and $F_o - F_c$ electron density maps contoured to 1σ and 3σ, respectively. The model was modified to fit the density and refined in an iterative manner until a final R factor of 19.8% and an R_{free} of 25.3% were reached.

The 2B4−clopidogrel complex structure was determined by molecular replacement in Phaser using the same search model that was used for the ticlopidine structure. The solution was found in space group $P3$, containing 70.7% solvent assuming four monomers per asymmetric unit. The data were uploaded to the UCLA twinning server and determined to have a twin fraction of 0.43 (*37*, *38*). The initial model was subjected to rigid body refinement and a restrained refinement using REFMAC with the amplitude-based twin refinement and noncrystallographic symmetry options enabled. Model building and refinement were performed as described above until a final R factor of 17.8% and an R_{free} of 23.4% were reached. The noncrystallographic symmetry restraints were slowly released during this process. Structure refinement statistics are summarized in Table 1.

Active Site Cavity Volume Calculations. Active site cavity volumes were calculated using Voidoo (*39*). Ten cycles of cavity

Table 1: X-ray Data Collection and Refinement Statistics

	ticlopidine	clopidogrel
Crystal Data		
space group	$P3_221$	$P3$
unit cell dimensions		
a, b, c (Å)	93.5, 93.5, 137.1	234.5, 234.5, 57.32
α, β, γ (deg)	90, 90, 120	90, 90, 120
Data Collection		
X-ray source	SSRL beamline 11-1	SSRL beamline 11-1
wavelength (Å)	0.98	0.98
resolution range (Å)	69.67−2.67	76.76−3.10
total no. of observations	144860	249852
no. of unique observations ($F > 0$)	20223	62529
completeness (%)[a]	99.8 (100.0)	97.7 (98.6)
redundancy[a]	7.2 (7.2)	4.0 (3.9)
I/σ[a]	4.9 (1.7)	4.7 (1.6)
R_{merge} (%)[a,b]	10.1 (41.6)	13.0 (43.2)
Refinement Statistics		
R factor (%)[c]	19.80	17.77
R_{free} (%)[c]	25.30	23.41
rmsd for bond lengths (Å)	0.010	0.019
rmsd for bond angles (deg)	1.406	1.936
no. of atoms		
protein[d]	3743 (66.4 Å^2)	14920 (42.3 Å^2)
heme[d]	43 (49.6 Å^2)	172 (28.3 Å^2)
ligand[d]	17 (69.4 Å^2)	84 (104.0 Å^2
Cymal-5[d]	68 (96.6 Å^2)	not applicable
cholate[d]	80 (117.2 Å^2)	not applicable
water[d]	31 (62.5 Å^2)	176 (28.5 Å^2)

[a]Values for the highest-resolution shell are in parentheses. [b]$R_{merge} = \sum_h\sum_i|I_h - I_{hi}|/\sum_h\sum_i I_{hi}$, where I_h is the mean of I_{hi} observations of reflection h. [c]R factor and $R_{free} = \sum||F_o| - |F_c||/\sum|F_o| \times 100$ for 95% of the recorded data and 5% of the data, respectively. [d]Average B factors are in parentheses.

detection using a probe-occupied volume were performed with a probe radius of 1.40 Å.

Ligand Docking. Ligand docking was performed by two methods. In one method, Autodock4 (*40*) was used to allow free movement of the ticlopidine in the 2B4 active site, but the protein side chains were fixed in place. Prior to docking, the 2B4−ticlopidine complex coordinate file was modified. Any residues not modeled into the experimental electron density were added using COOT, and ticlopidine, Cymal-5, and 232-chol were removed from the file. The Autodock4 script used to simulate ligand binding added all hydrogen atoms to the protein and ligand PDB files, removed any water molecules, and was run with default settings. Small molecule charges were set to Gasteiger. Charges found on the heme were modified using a separate script citing values previously reported (*41*). The docking experiment included 100 events using a grid size of 70 Å × 70 Å × 70 Å with 0.375 Å spacing.

The second method used simulated annealing (*42*), which applied NMR-derived distance restraints from the paramagnetic relaxation experiments as described for other systems (*43*, *44*). Residues missing from the protein coordinate file were added using the homology modeling program Modeller (*45*). Ticlopidine was then manually docked in an arbitrary orientation in the X-ray crystal structure of 2B4 using PyMOL (*46*). Distance-restrained simulated annealing and energy minimization of 2B4 and ticlopidine were performed with Groningen MAchine for Chemical Simulation (GROMACS) version 4.07 (*47*). The 2B4−ticlopidine complex was simulated with the GROMOS96 53a6 force field (*48*) and the particle mesh Ewald (*49*) method for electrostatics. Ticlopidine was restrained using the NMR-calculated distances from Table 3 with a force constant of 600 kJ mol^{-1} nm^2. A time constant of 50 ps was applied to the distance restraint to allow the molecule to move in the active site during the simulation, because the NMR distances reflect multiple orientations of ticlopidine in the 2B4 active site. The molecule was then energy minimized using the conjugate gradient method to eliminate van der Waals contacts. The system was then heated to 800 K and cooled to 300 K in 150 ps and allowed to equilibrate for 100 ps at 300 K.

Protein Figures. All protein figures were generated using PyMOL (*46*).

Proton NMR and Longitudinal (T_1) Relaxation Measurements for Ticlopidine. For these studies, NMR experiments with ticlopidine in the presence of purified 2B4 were performed on a 600 MHz Bruker Avance III apparatus (Bruker Daltonics Inc., Billerica, MA) with a three-channel (^{1}H, ^{15}N, ^{13}C) cryoprobe as described previously (*27*, *50*−*52*). The NMR longitudinal relaxation was measured using a pulse sequence containing a 180° inversion pulse followed by a WATER suppression by GrAdient Tailored Excitation (WATERGATE) (*53*) or by an excitation sculpting pulse sequence (*54*). The NMR samples contained 5 μM 2B4 and 1.15 mM ticlopidine in 25 mM potassium phosphate (pD 7.0) with >99% D_2O with 1% d_4-methanol as a cosolvent for ticlopidine. The low-ionic strength buffer was necessary to prevent the drug from aggregating, which interfered with the NMR measurement. In addition, the NMR relaxation measurements were performed at a range of protein concentrations as described previously (*55*). However, the most sensitive and least error prone measurements were taken at a concentration of 5 μM P450 2B4 and 1.15 mM ticlopidine. NMR relaxation measurements at lower concentrations of P450 2B4 showed less sensitivity and greater errors, while measurements at higher concentrations of P450 2B4 were hindered by broadening of the ticlopidine peaks. The selected conditions also allowed ticlopidine to exchange rapidly between the bulk solvent and the 2B4 active site, which is also essential for the experiment (see pages 2 and 3 of the Supporting Information). Paramagnetic samples, in which heme iron is in the Fe^{3+} state, were prepared by purging for 2 h under argon in sealed 5 mm NMR tubes. Diamagnetic samples, in which the heme iron is in the Fe^{2+} state, were made when they were gently bubbled in carbon monoxide for 1 min. Then a small amount of dithionite was added to the sample under a flow of argon. As a measure of anaerobicity, BD Dry Anaerobic indicator strips for GasPak jar systems (BD Biosciences, San Jose, CA) were dipped in a dithionite solution prior to insertion of the strips into the NMR tube. A strip that turned blue during the NMR experiments was deemed contaminated with oxygen, and the experiment was repeated, because oxygen would introduce errors into the relaxation measurements.

Processing, Background Subtraction, and Deconvoluting NMR Spectra. NMR spectra were processed using iNMR (http://www.inmr.net). The NMR spectra were then translated into the ASCII text format and imported into Igor Pro version 6.1. The background and baseline were subtracted from NMR spectra using software written in the Python programming language (version 2.6.4) and integrated into Igor Pro version 6.1.

Table 2: Spectral Binding and Inhibition Studies[a]

	2B4dH			2B6dH		
drug	ΔA_{max} (OU μM^{-1})	K_s (μM)	K_i (μM)	ΔA_{max} (OU μM^{-1})	K_s (μM)	K_i (μM)
clopidogrel	0.05 ± 0.001	0.6 ± 0.06	0.36 ± 0.04	0.04 ± 0.005	0.1 ± 0.07	0.10 ± 0.01
ticlopidine	0.03 ± 0.008	1.3 ± 0.1	0.81 ± 0.10	0.02 ± 0.001	0.3 ± 0.13	0.14 ± 0.02

[a]Standard errors for a fit to the respective equations are shown. Results are representative of at least two independent determinations. OU stands for optical units.

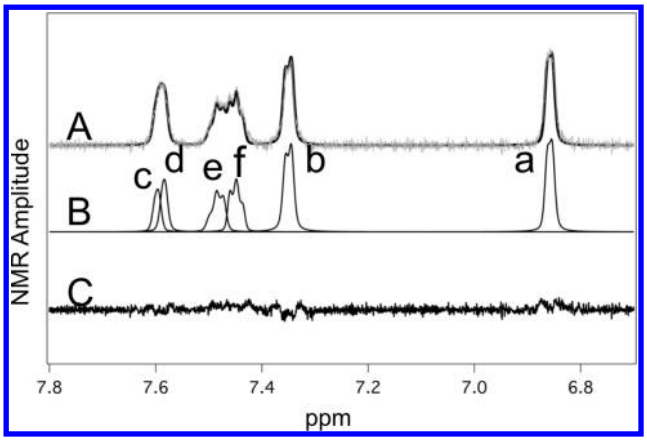

FIGURE 2: Fitting of NMR spectrum of ticlopidine in the presence of 5 μM reduced 2B4. (A) NMR spectrum (gray line) and simulated fit (black line) of ticlopidine in the presence of reduced 2B4 with the background subtracted. (B) Simulations of the individual NMR transitions that comprise the ticlopidine spectrum with lowercase letters denoting the proton assignments from Figure 1. (C) Residual between the simulated fit and the NMR spectrum.

The NMR spectra were then curve fit using methods that have been described previously (*56*−*59*). Curve fitting was accomplished in two steps. First, the positions of the peaks were estimated via analysis of the spectra under different conditions, including different protein concentrations and different solvent conditions (Figure S1 of the Supporting Information), and analysis of the NMR spectra by principal component analysis (PCA) as described previously (*60*−*62*). The latter PCA analysis was accomplished using software written in the Python programming language with the module Numpy and integrated into Igor Pro version 6.1. Using the peak positions determined from the previous analyses, the data were fit to a linear combination of Gaussian, Lorentzian, or Voigt line shapes (*56*−*58*, *63*) by using the multiple-peak fitting package (version 2.0) of Igor Pro version 6.1 and a least-squares fitting program written in Python using Numpy.

Singular-Value Decomposition Analysis of the NMR Relaxation Measurements. Singular-value decomposition (SVD) analysis was used to measure the amplitudes of the NMR peaks using reference peak standards simulated from the curve fitting (Figure 2), which was similar to other SVD methods using prior knowledge of the NMR spectra (*64*−*66*). The SVD algorithm was written in Python programming language (version 2.6.4) using Numpy and integrated into the scientific analysis package Igor Pro version 6.1. In terms of accurately measuring peak amplitude, this method produced signal-to-noise ratios far superior to those produced by other methods such as measuring the peak amplitude directly or integrating the peak. The SVD-derived amplitudes were then fit using a single-exponential function in Igor Pro version 6.1.

Calculating Distances of Ticlopidine Protons from the 2B4 Heme Iron. The paramagnetic relaxation rate (R_P) was calculated by taking the differences between oxidized and reduced P450. This relationship can be represented mathematically; $R_P = R_{Fe^{3+}} - R_{CO-Fe^{2+}}$, where R_P is the paramagnetic relaxation rate, $R_{Fe^{3+}}$ is the relaxation rate of the oxidized P450, and $R_{CO-Fe^{2+}}$ is the relaxation rate of reduced P450 with carbon monoxide. The paramagnetic relaxation rate was related to distance by the Solomon−Bloembergen equation (eq 1) (SI units) (*67*)

$$R_P = \alpha \frac{2}{15}\left(\frac{\mu_0}{4\pi}\right)^2 \frac{\gamma_N^2 g_e^2 \mu_B^2 S(S+1)}{r_{app}^6} \left[\frac{\tau_C}{1+(\omega_N-\omega_E)^2} + \frac{3\tau_C}{1+\omega_N^2\tau_C^2} + \frac{6\tau_C}{1+(\omega_N+\omega_E)^2\tau_C^2}\right] \quad (1)$$

where α is the fraction of ligand bound, μ_0 is the magnetic permeability of free space, γ_N is the nuclear gyromagnetic ratio, g_e is the electronic g factor, μ_B is the Bohr magneton, r is the apparent time-averaged electron−nuclear distance, τ_C is the correlation time for the nuclear−electron interaction vector, S is the electronic spin quantum number, and ω_N and ω_E are the radial frequencies of the nucleus and electron, respectively. The $\mu_0/4\pi$ term of the equation was used to convert the equation to SI units, which was absent in older equations because they were originally based on centimeter gram second units (*67*). The fraction of ligand (α) was calculated from the equation $\alpha = [EL]/[L_0] = [E_0]/(K_D + [L_0])$, where [EL] is the concentration of the enzyme−ligand complex, $[L_0]$ is the total concentration of substrate, and K_D is the dissociation constant. The $S(S+1)$ term accounts for the spin state of the P450. For mixed spin state systems (*26*), it was calculated using the equation $S(S+1) = 8.75 f_{HS} + 0.75 f_{LS}$, where f_{HS} and f_{LS} are the fractions of high spin and low spin, respectively, which were determined by least-squares fitting 2B4 standards of an absolute absorbance spectrum of 2B4 in the presence of a saturating level of ticlopidine as previously described (*31*, *68*) and shown in Figure S1 of the Supporting Information. A correlation time for the nuclear−electron interaction vector (τ_C) of 3×10^{-10} was used in the calculation, and it is the average value of P450 species under several conditions (*27*, *69*). The ω_N term is equal to 3.77×10^9 rad/s, and ω_E is equal to -2.48×10^{12} rad/s.

Effect of Ligand Dynamics on R_P, r_{app}, and r_{avg}. Because of ligand dynamics and the fast exchange requirement for these measurements, the distances calculated from this analysis are not likely to represent absolute distances, but time-averaged distances weighted toward the shortest distance. The time averaging of the distances of mobile nuclei and paramagnetic species was accomplished using the ensemble approach (*70*, *71*). The time-dependent ensemble averaging equations of R_P and r_{app} are

Table 3: Paramagnetic Relaxation and Calculated Distances of 1.15 mM Ticlopidine in the Presence of 5 μM 2B4

peak	$R_{Fe^{3+}}$ (s^{-1})	$R_{Fe^{2+}-CO}$ (s^{-1})	R_P (s^{-1})	r_{app}[a] (Å)	$r_{X\text{-}ray}$[b] (Å)	$r_{X\text{-}ray}$[c] (Å)
a	2.03 ± 0.22	0.77 ± 0.04	1.26 ± 0.22	7.54 ± 0.22	3.34	10.49
b	2.27 ± 0.17	0.89 ± 0.06	1.38 ± 0.18	7.43 ± 0.16	4.92	12.57
c	2.86 ± 0.09	1.00 ± 0.03	1.87 ± 0.10	7.06 ± 0.06	11.95	4.87
d	2.72 ± 0.07	1.11 ± 0.03	1.61 ± 0.08	7.23 ± 0.06	9.86	8.77
e	3.16 ± 0.29	1.00 ± 0.05	2.16 ± 0.29	6.89 ± 0.16	13.01	7.15
f	2.81 ± 0.21	1.05 ± 0.07	1.76 ± 0.22	7.13 ± 0.15	12.16	8.68

[a]Calculated time-averaged distances between the ticlopidine protons and the heme iron. The K_D used for the distance calculation was 5.95 ± 1.20 μM (Figure S2E of the Supporting Information). Concentrations of 58% LS and 42% HS were calculated using least-squares fitting in the presence of saturating 64 μM ticlopidine (Figure S2F of the Supporting Information). The error reflects uncertainty in the calculation and not a maximum and minimum distance of protons from the heme (*78*). [b]Distances to the heme iron determined by adding protons to the ticlopidine molecule in the X-ray crystal structure thiophene down orientation. [c]Distances to the heme iron determined by adding protons to the ticlopidine molecule in the X-ray crystal structure chlorophenyl down orientation.

shown in eq 2

$$R_P = \sum_0^n \frac{\Delta t_n}{t} R_n = \sum_n^n f_t R_n$$

$$\propto {r_{app}}^{-6} = \sum_0^n \frac{\Delta t_n}{t} {r_n}^{-6} = \sum_0^n f_t {r_n}^{-6} \quad (2)$$

where Δt_n is the fraction of time, t is the total time, and f_t is the fraction of time at an individual distance. The top part of eq 2 shows that the paramagnetic relaxation rate (R_P) is linearly related to the individual relaxation rates, whereas r_{app} has r^6 dependence in the bottom part. The effect of this is that r_{app} will be skewed toward the shortest distance, whereas the paramagnetic relaxation rate will remain linear. For a molecule that fluctuates, the average distance (r_{avg}) is quite different from r_{app} and was calculated using eq 3.

$$r_{avg} = \sum_0^n \frac{\Delta t_n}{t} r_n = \sum_0^n f_t r_n \quad (3)$$

Like R_P, r_{avg} is linear with respect to the individual distances (r_n) in contrast to r_{app}. To improve our understanding of the time averaging effect of r_{app}, a simulation of r_{app}, r_{avg}, and R_P is presented in the Supporting Information.

RESULTS

Spectral Binding and Enzyme Inhibition. Clopidogrel and ticlopidine both induced type I difference spectra with a peak at ~388 nm and a trough at ~420 nm (Figure S2 of the Supporting Information). 2B6 and 2B4 exhibited similar ΔA_{max} values with clopidogrel and ticlopidine. Compared with 2B6, 2B4 showed approximately 4- and 6-fold higher K_s values with ticlopidine and clopidogrel, respectively (Figure S2 of the Supporting Information and Table 2). The K_i values were determined for competitive inhibition of 2B6 and 2B4 by clopidogrel and ticlopidine using 7-EFC at concentrations of up to 150 μM and drug concentrations of 0−5 μM. P450 2B4 exhibited 4- and 6-fold higher K_i values than 2B6 with clopidogrel and ticlopidine, respectively (Figure S3 of the Supporting Information and Table 2).

2B4−Ticlopidine Complex. The protein backbone of the 2B4−ticlopidine complex is very similar to that of the closed

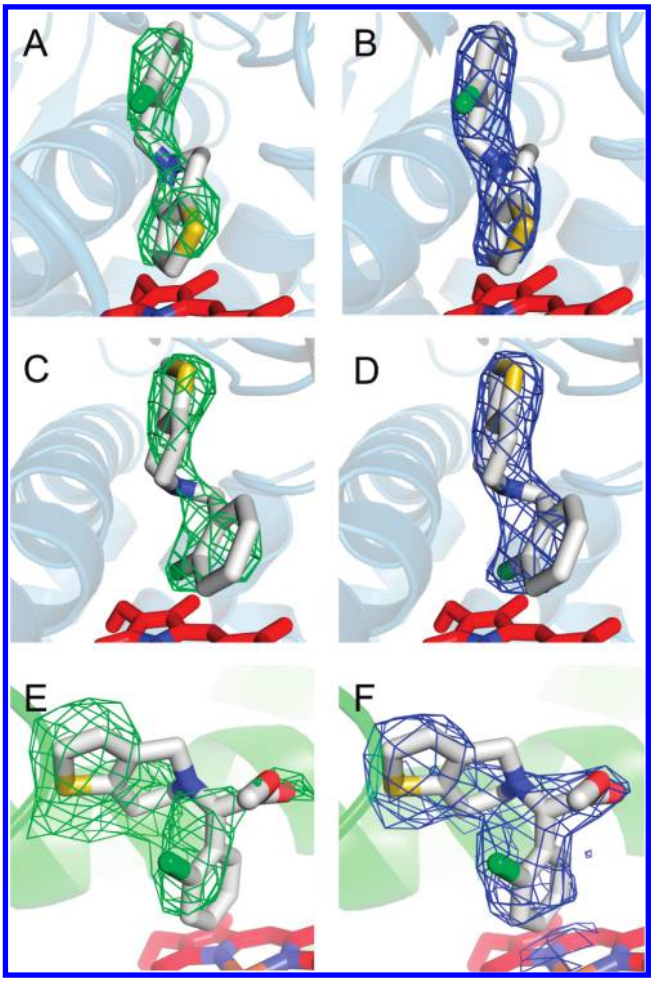

FIGURE 3: Electron density maps for ticlopidine and clopidogrel. (A) An unbiased $F_o - F_c$ simulated annealing omit map for ticlopidine contoured at 3σ shows two lobes of electron density above the plane of the heme with the thiophene down orientation for the ligand. (B) The $2F_o - F_c$ map for the thiophene down orientation of ticlopidine contoured at 1σ after refinement. (C) The same $F_o - F_c$ omit map from panel A is shown with the alternative chlorophenyl down orientation of ticlopidine. (D) The $2F_o - F_c$ map for the chlorophenyl down orientation of ticlopidine contoured at 1σ after refinement. (E) An unbiased $F_o - F_c$ simulated annealing omit map for clopidogrel contoured at 3σ shows two large lobes and one smaller lobe of electron density above the plane of the heme. (F) The $2F_o - F_c$ map for clopidogrel contoured at 1σ shows clearly shows its orientation after refinement.

2B4−4-CPI complex (*5*) that was used as a molecular replacement search model (Figure S4 of the Supporting Information). With an rmsd of 0.37 Å over all C_α atoms, the largest differences occur in the C−D loop and helix I. Changes in side chain orientations compared with the molecular replacement model were fit into the electron density maps with little effort (Figure S5A of the Supporting Information). Additionally, two Cymal-5 molecules and a partial 232-chol molecule were modeled into the electron density. This 232-chol molecule mediates a crystallographic 2-fold axis near helix F′. Two lobes of electron density of approximately the same size and consistent with ticlopidine sat above the plane of the heme. Initially, the substrate was modeled with the thiophene ring closest to the heme (Figure 3A,B), in accordance with metabolic data for human P450 2B6 (*72*). However, during refinement, ticlopidine could also fit the density when flipped "upside down" to point the chlorophenyl moiety toward the heme (Figure 3C,D) without generating negative

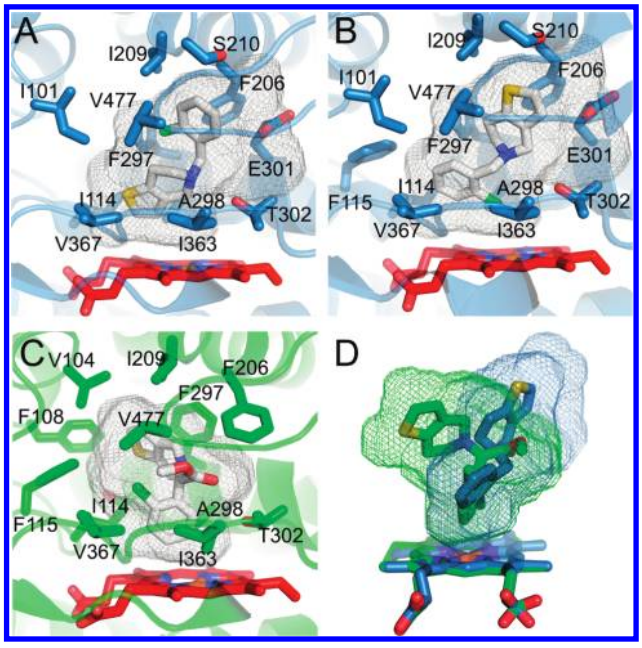

FIGURE 4: Ribbon and stick diagrams showing the active site of 2B4. The gray mesh in each panel shows the active site cavity volume as calculated by Voidoo in Materials and Methods. (A) Residues within a 5 Å radius of the ligand make up the ticlopidine binding site. In the thiophene down orientation, ticlopidine makes contact with Ile 101, Ile 114, Phe 115, Phe 206, Ile 209, Ser 210, Phe 297, Ala 298, Glu 301, Thr 302, Ile 363, Val 367, and Val 477. The active site cavity is long and flat, following the shape of the ticlopidine molecule from the D ring of the heme toward helices F and G. Heme is shown as red sticks and ticlopidine as white sticks. (B) The chlorophenyl down orientation of ticlopidine sits in the same pocket but has an additional contact with Phe 115. (C) Residues within a 5 Å radius of the ligand make up the clopidogrel binding site. These residues are Val 104, Phe 108, Ile 114, Phe 115, Phe 206, Ile 209, Ser 294, Phe 297, Ala 298, Thr 302, Ile 363, Val 367, and Val 477. The active site cavity is roughly globular with a protrusion along helix I where the thiophene ring sits. Heme is shown as red sticks and clopidogrel as white sticks. (D) An overlay of meshes highlights the differences in the active site cavities of the two complexes. The ticlopidine and clopidogrel complexes are colored blue and green, respectively.

peaks in $F_o - F_c$ maps. In light of these results, ticlopidine was modeled into the electron density maps in two orientations. In one orientation, the thiophene ring occupies the lobe of density closest to the heme (Figure 4A). In this case, the sulfur atom is 6.6 Å from the heme iron, while the carbon bearing proton a (Figure 1) is closest (distance of 4.3 Å). In the second orientation, the chlorophenyl group occupies the lobe of electron density closest to the heme (Figure 4B). The chlorine atom moves closest to the heme iron, with a distance of 4.1 Å. In both orientations, ticlopidine makes contact with Ile 101, Ile 114, Phe 206, Ile 209, Ser 210, Phe 297, Ala 298, Glu 301, Thr 302, Ile 363, Val 367, and Val 477, which are found within a 5 Å radius of the ligand. The chlorophenyl down orientation has an additional contact with Phe 115.

2B4−Clopidogrel Complex. To further explore the interactions of 2B4 with antiplatelet drugs, we crystallized the enzyme in the presence of clopidogrel. The structure of the 2B4−clopidogrel complex also shares a high degree of similarity with the structure of the 2B4−4-CPI complex (Figure S4 of the Supporting Information). A structural alignment of the entire backbone yields an rmsd of 0.32 Å, with the largest differences occurring in the C−D and H−I loops and helix I. Despite the modest resolution, differences in side chain orientations were easily identified in the electron density maps (Figure S5B of the Supporting Information). Clopidogrel was found to occupy a trilobed region of electron density (Figure 3D,E) above the heme plane, with the chlorophenyl group most closely approaching the heme. The closest points of clopidogrel are two carbon atoms, each 3.6 Å from the heme iron. The thiophene ring points in the opposite direction along helix I compared with the chlorophenyl down orientation of ticlopidine (Figure 4C,D) and is sequestered by a number of phenylalanine residues (Phe 108, Phe 115, Phe 206, and Phe 297) on the B−C loop and helices F and I as well as Val 104, Ile 114, Ile 209, and Ser 294. The remaining residues that come into contact with the ligand are Ala 298, Thr 302, Ile 363, Val 367, and Val 477. The carboxymethyl moiety is not within hydrogen bonding distance of any polar side chain or main chain atoms.

Ligand Docking. To further evaluate the two ticlopidine orientations modeled into the electron density maps, the molecule was docked into the 2B4−ticlopidine complex active site cavity by two separate methods. During the performance of 100 Autodock runs where protein side chains were fixed in place, two clusters of poses for ticlopidine were observed. The most populated cluster contained 95 poses, all with a mean binding energy of −7.79 kcal/mol. These poses put the chlorophenyl ring closest to the heme in an orientation that is consistent with the chlorophenyl down orientation observed in the X-ray crystal structure (Figure S6A of the Supporting Information), although the thiophene ring is rotated ~180° with respect to the chlorophenyl ring. The other five poses occupied the second cluster and had mean binding energies ranging from −7.77 to −7.76 kcal/mol. These poses all placed the thiophene ring closest to the heme with the chlorophenyl ring above it (Figure S6B of the Supporting Information). However, because of bond rotations, this cluster does not correlate with the thiophene down orientation from the crystal structure.

The binding of ticlopidine was also explored using distance-restrained simulated annealing. The final 10 preferred orientations deduced from the simulation (Figure S6C of the Supporting Information) position ticlopidine with the chlorophenyl ring closest to the heme in an orientation that is consistent with both the X-ray crystal structure chlorophenyl down orientation and the predominant cluster using Autodock.

Assigning and Deconvoluting the Ticlopidine Proton NMR Spectrum in the Presence of 2B4. Proton NMR spectra of ticlopidine were recorded in the presence and absence of 2B4. The NMR peak assignments of ticlopidine are described in detail in the Supporting Information (pages 1 and 2) but are similar to assignments made previously (*73*, *74*). In the presence of 2B4, the peaks of the ticlopidine NMR spectrum were shifted and broadened (Figure S1 of the Supporting Information). Several of the peaks overlap significantly, making measurement of T_1 relaxation of individual peaks difficult. Therefore, the spectra were curve fit using a linear combination of Gaussian and Lorentzian line shapes (*56*, *58*), which approximates a Voigt function.

The spectrum with the background subtracted (Figure 2A) and the least-squares fit of simulated peaks (Figure 2B) had a correlation of 0.991. The approximate positions of the peaks were determined by observation of the shifts and broadening under different solvent conditions and different protein concentrations (Figure S3 of the Supporting Information and data not shown). The lack of peaks in the residual between fit and the data (Figure 2C) shows that the fit represents the data accurately.

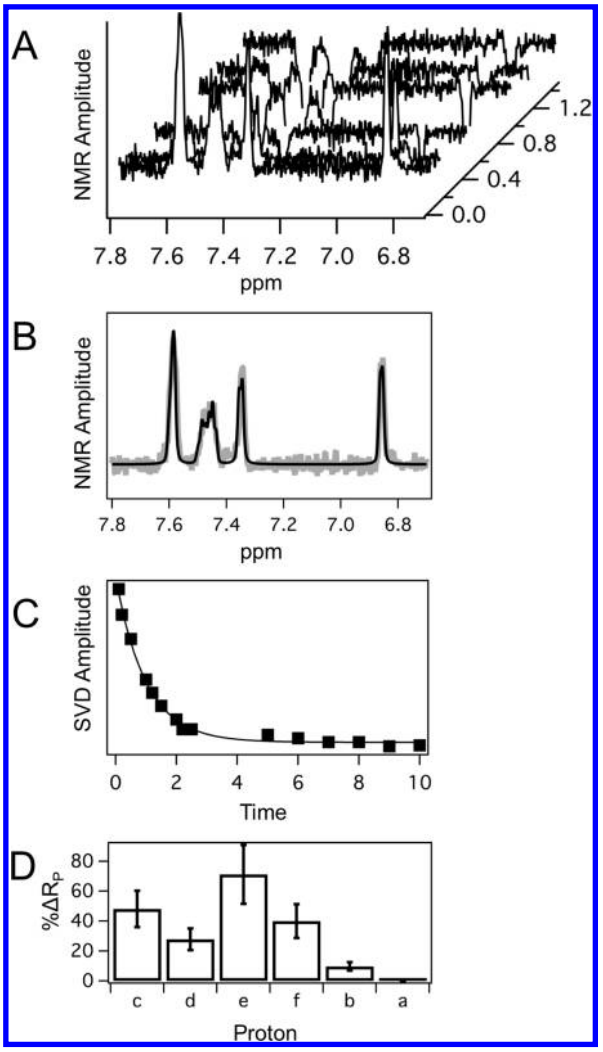

FIGURE 5: NMR relaxation of 1.15 mM ticlopidine in the presence of 5 μM reduced 2B4. (A) Waterfall graph of the 1D proton NMR spectra at various inversion recovery times with the background and baseline subtracted. (B) 1D proton NMR spectrum (gray line) at an inversion recovery time of 10 s with its fit colored black. (C) SVD analysis of the highly overlapping aromatic chlorophenyl proton peak labeled e as a function of inversion recovery time. (D) Relative differences in paramagnetic relaxation (R_P) of ticlopidine protons. The bar graph shows the percent difference in R_P with respect to aromatic proton a of the thiophene ring, which showed the weakest paramagnetic relaxation effect. Error bars indicate the variation calculations.

NMR Relaxation of Ticlopidine in the Presence of 2B4. NMR relaxation of ticlopidine protons was used to explore the orientation of ticlopidine in the 2B4 active site in solution (*26*). Figure 5 shows the results of the NMR relaxation of ticlopidine in the presence of reduced 2B4. A waterfall representation of individual one-dimensional (1D) proton NMR spectra that comprise the NMR relaxation experiment (Figure 5A) shows that at short inversion recovery times the peaks are positive but decrease in magnitude as the inversion recovery time is increased. At long inversion recovery times, the absolute amplitude is similar to that at short inversion recovery times, but in the opposite direction. The 1D proton NMR spectra and fit at inversion recovery time of 10 s (Figure 5B) were fit by a least-squares method (*56*, *58*−*60*, *63*) using the simulated peaks from Figure 2. In all cases, the correlation values of the fits were ≥0.97. Using the simulated peaks and inversion NMR spectra, the inversion recovery time was analyzed using the SVD method. As an example of the robustness of this method, the SVD amplitude of the highly overlapping aromatic chlorophenyl proton labeled e (Figures 1 and 2) is shown as a function of inversion recovery time (Figure 5C). The curve was fit to a single-exponential function and had a χ^2 of 3.24×10^{-5}, suggesting a good fit.

The relaxation rates of 1.15 mM ticlopidine in the presence of 5 μM 2B4 were deduced from SVD analysis (Table 3). The first two columns show the relaxation rates for oxidized Fe^{3+} 2B4 and reduced CO Fe^{2+} 2B4. The calculated paramagnetic relaxation (R_P) values are listed in column 3 and vary ~2-fold between protons. Using the Solomon−Bloembergen equation and the treatment described in Materials and Methods, the apparent time-averaged distances (r_{app}) can be calculated. Because of the r^6 distance dependence, chemical equivalence, and time averaging, the r_{app} values are significantly less dispersed and less sensitive to orientation and position than R_P. For the sake of comparison, the last column in Table 3 lists the distances deduced from the X-ray crystal structure ($r_{X\text{-}ray}$) to the heme iron. Because ticlopidine exhibits only two orientations in the X-ray crystal structure and is likely to be mobile under the conditions used for the NMR analysis, the X-ray crystal structure shows a significantly higher level of dispersion of the proton distances than the calculated distances from NMR. The disparity between these measurements is explained in more detail in the Discussion and the Supporting Information (pages 3 and 4).

Because of the higher sensitivity of R_P with respect to the orientation and position of ticlopidine, these rates were analyzed (Figure 5D and Figure S7 of the Supporting Information) with respect to the R_P of proton a (Figure 1), which relaxes slower than the other protons in the presence of 2B4. The proton labeled e, which corresponds to a proton on the chlorophenyl ring, shows the faster relaxation, which is 71% faster than that of proton a on the opposite end of the molecule. In contrast, the proton adjacent to proton a on the thiophene ring proton (proton b) had an R_P that was only 10% greater. From this analysis, it becomes apparent that the protons on the chlorophenyl ring are relaxed more rapidly than those on the thiophene ring. Thus, the preferred orientation of ticlopidine is that with the chlorophenyl ring oriented toward the heme.

DISCUSSION

The two structures presented here represent the first 2B complexes with non-imidazole ligands. Clopidogrel and ticlopidine, which lack coordination of nitrogen to the heme iron, have more freedom of rotation in the active site, which we expected would influence their binding modes. The multiple conformations of ticlopidine are consistent with this hypothesis and with metabolism studies that report multiple products from oxidation by various mammalian P450 species (*14*, *16*, *17*, *75*). Analysis of previous structures (*4*−*7*) largely focused on the discussion of highly mobile secondary structural elements that could reposition themselves in response to imidazole inhibitors of various sizes. In contrast, comparisons of the ticlopidine and clopidogrel complexes show a similar protein backbone (Figure S4 of the Supporting Information) but highlight the ability of the enzyme to accommodate ligands through rearrangement of active site residues (Figure 4 and Figure S5 of the Supporting Information).

In the clopidogrel complex, Phe 206 enters the active site and sits above the B ring of the heme. To make room for ticlopidine, this residue rotates out of the active site and points toward helix I. A similar result is observed with Phe 297. In the ticlopidine

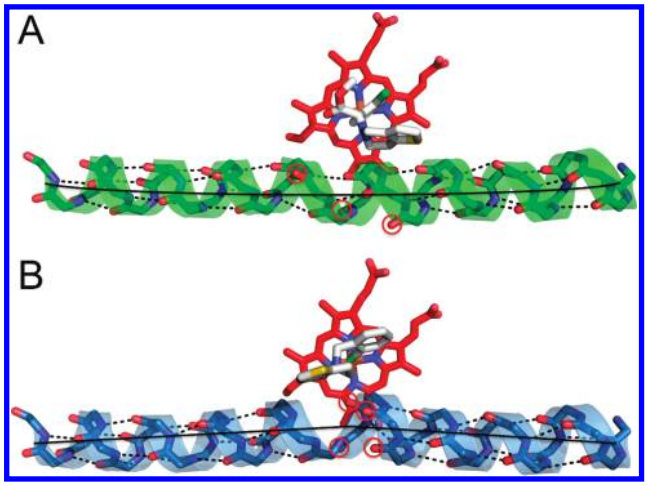

FIGURE 6: Ribbon and stick diagram showing the different placements of helix I. (A) In the 2B4−clopidogrel complex, helix I is slightly curved from end to end. Main chain helical contacts are lost at three points. The main chain oxygens of Phe 296, Gly 299, and Glu 301 are circled in red where these contacts are broken. The black line highlights the curvature of the helix. (B) In the 2B4−ticlopidine complex, helix I shows a kink beginning at residue 296 where the traditional n, $n + 4$ hydrogen bonding pattern of the helix diverges. The main chain oxygens of Phe 296, Phe 297, Ala 298, and Gly 299 are circled in red. The black lines highlight the kink in the helix.

complex, Phe 297 points into the active site above the A ring of the heme. Because the thiophene ring of clopidogrel occupies this space in the other structure, the side chain of Phe 297 rotates out of the active site and points up toward helix F. These small differences result in active site cavity volumes of 415.4 and 373.5 Å^3 for the clopidogrel and ticlopidine complexes, respectively (Figure 4D).

In addition to side chain differences between the two complexes, there are small changes in main chain interactions near the active site. Immediately following Leu 295, helix I of the clopidogrel complex is pushed toward helix E to accommodate the binding of the thiophene ring of clopidogrel. In this region, Phe 296 loses its main chain interaction with Thr 300, but standard helical interactions resume immediately afterward until they are broken again for helical hydrogen bonding partners Gly 299 and Thr 303, and Glu 301 and Thr 305. Instead of maintaining the canonical secondary structure hydrogen bonding pattern, the distorted main chain oxygens of Phe 296, Gly 299, and Gly 301 are in position to possibly hydrogen bond with the nearby side chains of Thr 300, Thr 303, and Thr 305, respectively, to regain the energy lost from the breakage of the helical pattern. These repositioned main chain interactions help account for the rotation of Phe 297 out of the active site to make room for the thiophene ring and also result in a gradual bowing of helix I from one end to the other (Figure 6A). In contrast, in the ticlopidine complex, helix I is kinked toward helix E beginning at Phe 296, where the main chain carbonyls of Phe 296, Phe 297, Ala 298, and Gly 299 lose their hydrogen bonding partners of the main chain amides from Thr 300, Glu 301, Thr 302, and Thr 303, respectively (Figure 6B). In both cases, helix I breaks the standard hydrogen bonding pattern of an α-helix where the carbonyl oxygen of residue n interacts with the amide nitrogen of residue $n + 4$. This phenomenon is also observed in the 4-CPI complexes of 2B4 (*5*) and 2B6 (*8*) and to a lesser extent in the 1-CPI complex of 2B4 (*6*). Helix I is also kinked in the structure of the 2B4−bifonazole complex, but in a different manner (*7*). Traditional hydrogen bonding is consistent throughout helix I of the 1-PBI complex (*4*). While these subtle variations among the clopidogrel, ticlopidine, 4-CPI, and 1-CPI complexes are less pronounced than the large structural rearrangements seen in the 1-PBI and bifonazole complexes, these distortions of helix I highlight the variable mechanisms at the disposal of 2B enzymes to accommodate ligands and substrates of varying geometries.

The similarities between these two 2B4−thiophene drug complexes and the previously determined CPI structures (*5*, *6*) raise questions about the role that the structural plasticity of 2B4 found in X-ray crystal structures with bifonazole (*7*) and 1-PBI (*4*) plays in the enzyme's natural environment. 2B4 appears to have two modes of adapting to the ligands it encounters: global and local plasticity. With large imidazole inhibitors, the iron−nitrogen coordination in the active site results in protein conformations that are driven by the ligand. For example, isothermal titration calorimetry showed that the binding of bifonazole or 1-[2-(benzyloxy)ethyl]imidazole to 2B4 is entropically unfavorable (but overall is favorable because of large negative enthalpies), indicating that the ligands are introducing strain on the active site (*7*, *29*), causing it to open to accommodate the large inhibitor volumes. The wide open conformation seen in the structure of the 2B4−bifonazole complex (*7*) is consistent with this model. The tight interaction between the heme and ligand and the variability between the sizes of these molecules cause the protein to reorganize its secondary structural elements to accommodate these ligands, resulting in global plasticity.

In contrast to imidazole-based inhibitors, clopidogrel and ticlopidine do not bind to the heme. The weaker binding is reflected in their higher K_s values (Table 2). For reference, 4-CPI, bifonazole, and 1-PBI exhibit K_s values of 0.04, 0.13, and 0.23 μM, respectively (*4*). Compared with the 2B4 complexes of 4-CPI (*5*) and 1-CPI (*6*), the ligands in the thiophene complexes appear to be conforming to the protein. Despite their similar molecular structures, the additional carboxymethyl group of clopidogrel (Figure 1) causes the thiophene ring to adopt an orientation different from either observed in the ticlopidine complex (Figure 4). However, it is apparent that the protein undergoes far less rearrangement to bind these smaller compounds (4-CPI, 1-CPI, ticlopidine, and clopidogrel) compared to that observed with the large imidazoles. This brings up the possibility that one specific 2B4 orientation (or a small number) may be suitable for binding multiple ligands that are similar in size, a phenomenon that has already been observed in 2A6 (*76*, *77*). The movements that are observed in these cases are limited to shifts in side chain orientation (Figure 4 and Figure S5 of the Supporting Information) and deformation of helix I (Figure 6). This local plasticity in the active site is likely how 2B enzymes behave with a majority of compounds until they encounter ligands with unusually large volumes, unique stereochemistry, or other features that require the protein to displace secondary structural elements for oxidation to occur. Adjusting ligand orientation over protein conformation makes sense energetically, because it takes much less energy for a molecule to reorient than for the protein secondary or tertiary structure to rearrange. However, having structural flexibility at their disposal aids in allowing 2B enzymes to accommodate their wide array of substrates.

Despite their differences in binding, clopidogrel and one ticlopidine orientation place the aromatic chlorophenyl group closest to the 2B4 heme. The positioning of clopidogrel and the chlorophenyl down orientation of ticlopidine are consistent with a recent study that identified two ticlopidine metabolites that are

formed via a novel chlorophenyl epoxidation pathway in rat liver microsomes (*16*), whereas there are no reports of chlorophenyl ring oxidation metabolites from clopidogrel. Alternatively, the thiophene down orientation of ticlopidine supports several studies that show formation of thiolactones or thiophene *S*-oxides from ticlopidine and clopidogrel by 2C19 (*14*, *17*) or from clopidogrel by 1A2 and 2B6 (*17*). However, this does not appear to be the favored conformation in solution in 2B4. Ligand dynamics deduced from analysis of NMR relaxation of ticlopidine reveals a possible structural mechanism whereby 2B4 can accomplish thiophene oxidation reactions, while still maintaining a chlorophenyl down orientation most of the time.

The 71% higher paramagnetic relaxation rates observed for protons on the chlorophenyl ring suggest that the molecule is preferentially oriented with the chlorophenyl ring closer to the heme. The molecule is in "fast exchange" and likely adopts multiple orientations within the 2B4 active site. The averaging of these orientations makes the calculated distances (r_{app}) seem parallel with a maximum difference in distances of 0.65 Å. The time averaging effect could also explain why the distances of ligands bound to 1A2 (*27*) and 73A1 (*52*) were less dispersed than expected. However, the X-ray crystal structure and the molecular docking simulations show that ticlopidine orientations that are perpendicular to the heme. Using the equations in Materials and Methods, the amount of movement required for ticlopidine to have an only 0.65 Å difference in r_{app} was calculated. In the calculation, ticlopidine was assumed to oscillate between two perpendicular orientations, which places the a proton at either of two distances [i.e., 10.49 and 3.34 Å (Table 3)]. Interestingly, to have a difference in r_{app} of 0.65 Å, the molecule has to be oriented with the thiophene ring toward the heme only ~27% of the time. In this model, the chlorophenyl ring is still primarily oriented toward this heme but allows the thiophene ring to transiently interact with the heme where it can form the reported thiolactone and thiophene *S*-oxide metabolites as well.

To date, there are no publications about the metabolism of clopidogrel or ticlopidine by 2B4. However, our ongoing studies have shown that both 2B4 and 2B6 can form multiple metabolites from ticlopidine, with time courses that deviate rapidly from linearity and are consistent with mechanism-based inactivation. Compared with 2B6, 2B4 catalyzes more N-oxidation and less oxidation of the thiophene ring.[2] These unpublished results are consistent with our analysis of the data gathered from X-ray crystallography, NMR, and computational experiments regarding binding of ticlopidine to 2B4 as well as previous studies of thiophene drug metabolism in other P450 species (*14*, *16*, *17*, *75*). While our previous structural studies of 2B4 have focused on ligand-driven conformational flexibility (*4*−*7*, *29*), the results presented here emphasize how ligand dynamics affect the P450−ligand complex.

ACKNOWLEDGMENT

We thank Stephanie C. Huelga for assistance using Autodock. We also thank the staff at the Stanford Synchrotron Radiation Lightsource for assistance with data collection. The Stanford Synchrotron Radiation Lightsource is operated by Stanford University on behalf of the U.S. Department of Energy, Office of Basic Energy Sciences. The Stanford Synchrotron Radiation Lightsource is supported by the National Institutes of Health, the National Center for Research Resources, the Biomedical Technology Program, and the U.S. Department of Energy of Biological and Environmental Research.

SUPPORTING INFORMATION AVAILABLE

Results regarding NMR assignments of ticlopidine protons; results establishing fast exchange of ticlopidine protons; results of a simulation of r_{app}, r_{avg}, and R_P; NMR spectra of ticlopidine under various conditions (Figure S1); representative type I difference spectra for ticlopidine and clopidogrel binding to 2B4 and accompanying curve fits for K_s determination (Figure S2); curves used for the determination of K_i values for ticlopidine and clopidogrel (Figure S3); structural overlay of 2B4 complexes of ticlopidine, clopidogrel, and 4-CPI (Figure S4); typical electron density maps for side chains near the active site of ticlopidine and clopidogrel complexes of 2B4 (Figure S5); ticlopidine docking orientations in the 2B4 active site (Figure S6); relative NMR T_1 relaxation rates assigned to the chemical structure of ticlopidine (Figure S7); and effect of time averaging on r_{app}, r_{avg}, and R_P (Figure S8). This material is available free of charge via the Internet at http://pubs.acs.org.

REFERENCES

1. Johnson, E. F., and Stout, C. D. (2005) Structural diversity of human xenobiotic-metabolizing cytochrome P450 monooxygenases. *Biochem. Biophys. Res. Commun. 338*, 331–336.
2. Otyepka, M., Skopalik, J., Anzenbacherova, E., and Anzenbacher, P. (2007) What common structural features and variations of mammalian P450s are known to date? *Biochim. Biophys. Acta 1770*, 376–389.
3. Zhao, Y., and Halpert, J. R. (2007) Structure-function analysis of cytochromes P450 2B. *Biochim. Biophys. Acta 1770*, 402–412.
4. Gay, S. C., Sun, L., Maekawa, K., Halpert, J. R., and Stout, C. D. (2009) Crystal structures of cytochrome P450 2B4 in complex with the inhibitor 1-biphenyl-4-methyl-1*H*-imidazole: Ligand induced structural response through α-helical repositioning. *Biochemistry 48*, 4762–4771.
5. Scott, E. E., White, M. A., He, Y. A., Johnson, E. F., Stout, C. D., and Halpert, J. R. (2004) Structure of mammalian cytochrome P450 2B4 complexed with 4-(4-chlorophenyl)imidazole at 1.9 Å resolution: Insight into the range of P450 conformations and coordination of redox partner binding. *J. Biol. Chem. 279*, 27294–27301.
6. Zhao, Y., Sun, L., Muralidhara, B. K., Kumar, S., White, M. A., Stout, C. D., and Halpert, J. R. (2007) Structural and thermodynamic consequences of 1-(4-chlorophenyl)imidazole binding to cytochrome P450 2B4. *Biochemistry 46*, 11559–11567.
7. Zhao, Y., White, M. A., Muralidhara, B. K., Sun, L., Halpert, J. R., and Stout, C. D. (2006) Structure of microsomal cytochrome P450 2B4 complexed with the antifungal drug bifonazole: Insight into P450 conformational plasticity and membrane interaction. *J. Biol. Chem. 281*, 5973–5981.
8. Gay, S. C., Shah, M. B., Talakad, J. C., Maekawa, K., Roberts, A. G., Wilderman, P. R., Sun, L., Yang, J. Y., Huelga, S. C., Hong, W.-X., Zhang, Q., Stout, C. D., and Halpert, J. R. (2010) Crystal structure of a cytochrome P450 2B6 genetic variant in complex with the inhibitor 4-(4-chlorophenyl)imidazole at 2.0 Å resolution. *Mol. Pharmacol. 77*, 529–538.
9. Richter, T., Murdter, T. E., Heinkele, G., Pleiss, J., Tatzel, S., Schwab, M., Eichelbaum, M., and Zanger, U. M. (2004) Potent mechanism-based inhibition of human CYP2B6 by clopidogrel and ticlopidine. *J. Pharmacol. Exp. Ther. 308*, 189–197.
10. Sharis, P. J., Cannon, C. P., and Loscalzo, J. (1998) The antiplatelet effects of ticlopidine and clopidogrel. *Ann. Intern. Med. 129*, 394–405.
11. Farid, N. A., Kurihara, A., and Wrighton, S. A. (2010) Metabolism and disposition of the thienopyridine antiplatelet drugs ticlopidine, clopidogrel, and prasugrel in humans. *J. Clin. Pharmacol. 50*, 126–142.
12. Picard-Fraire, C. (1984) Pharmacokinetic and metabolic characteristics of ticlopidine in relation to its inhibitory properties on platelet function. *Agents Actions Suppl. 15*, 68–75.
13. Tuong, A., Boutssou, A., Paret, J., and Cuong, T. G. (1981) Metabolism of ticlopidine in rats: Identification and quantitative determination of some its metabolites in plasma, urine and bile. *Eur. J. Drug Metab. Pharmacokinet. 6*, 91–98.

[2]D. K. Dalvie et al., manuscript in preparation.

14. Ha-Duong, N. T., Dijols, S., Macherey, A. C., Goldstein, J. A., Dansette, P. M., and Mansuy, D. (2001) Ticlopidine as a selective mechanism-based inhibitor of human cytochrome P450 2C19. *Biochemistry 40*, 12112–12122.
15. Dalvie, D. K., and O'Connell, T. N. (2004) Characterization of novel dihydrothienopyridinium and thienopyridinium metabolites of ticlopidine in vitro: Role of peroxidases, cytochromes P450, and monoamine oxidases. *Drug Metab. Dispos. 32*, 49–57.
16. Ruan, Q., and Zhu, M. (2010) Investigation of bioactivation of ticlopidine using linear ion trap/orbitrap mass spectrometry and an improved mass defect filtering technique. *Chem. Res. Toxicol. 23*, 909–917.
17. Kazui, M., Nishiya, Y., Ishizuka, T., Hagihara, K., Farid, N. A., Okazaki, O., Ikeda, T., and Kurihara, A. (2010) Identification of the human cytochrome P450 enzymes involved in the two oxidiative steps in the bioactivation of clopidogrel to its pharmacologically active metabolite. *Drug Metab. Dispos. 38*, 92–99.
18. Hagihara, K., Nishiya, Y., Kurihara, A., Kazui, M., Farid, N. A., and Ikeda, T. (2008) Comparison of human cytochrome P450 inhibition by the thienopyridines prasugrel, clopidogrel, and ticlopidine. *Drug Metab. Pharmacokinet. 23*, 412–420.
19. Kalgutkar, A. S., Obach, R. S., and Maurer, T. S. (2007) Mechanism-based inactivation of cytochrome P450 enzymes: Chemical mechanisms, structure-activity relationships and relationship to clinical drug-drug interactions and idiosyncratic adverse drug reactions. *Curr. Drug Metab. 8*, 407–447.
20. Turpeinen, M., Nieminen, R., Juntunen, T., Taavitsainen, P., Raunio, H., and Pelkonen, O. (2004) Selective inhibition of CYP2B6-catalyzed bupropion hydroxylation in human liver microsomes in vitro. *Drug Metab. Dispos. 32*, 626–631.
21. Donahue, S. R., Flockhart, D. A., Abernethy, D. R., and Ko, J. W. (1997) Ticlopidine inhibition of phenytoin metabolism mediated by potent inhibition of CYP2C19. *Clin. Pharmacol. Ther. 62*, 572–577.
22. Tateishi, T., Kumai, T., Watanabe, M., Nakura, H., Tanaka, M., and Kobayashi, S. (1999) Ticlopidine decreases the in vivo activity of CYP2C19 as measured by omeprazole metabolism. *Br. J. Clin. Pharmacol. 47*, 454–457.
23. Scott, E. E., He, Y. A., Wester, M. R., White, M. A., Chin, C. C., Halpert, J. R., Johnson, E. F., and Stout, C. D. (2003) An open conformation of mammalian cytochrome P450 2B4 at 1.6-Å resolution. *Proc. Natl. Acad. Sci. U.S.A. 100*, 13196–13201.
24. Domanski, T. L., and Halpert, J. R. (2001) Analysis of mammalian cytochrome P450 structure and function by site-directed mutagenesis. *Curr. Drug Metab. 2*, 117–137.
25. Cameron, M. D., Wen, B., Allen, K. E., Roberts, A. G., Schuman, J. T., Campbell, A. P., Kunze, K. L., and Nelson, S. D. (2005) Cooperative binding of midazolam with testosterone and α-naphthoflavone within the CYP3A4 active site: A NMR T_1 paramagnetic relaxation study. *Biochemistry 44*, 14143–14151.
26. Cameron, M. D., Wen, B., Roberts, A. G., Atkins, W. M., Campbell, A. P., and Nelson, S. D. (2007) Cooperative binding of acetaminophen and caffeine within the P450 3A4 active site. *Chem. Res. Toxicol. 20*, 1434–1441.
27. Regal, K. A., and Nelson, S. D. (2000) Orientation of caffeine within the active site of human cytochrome P450 1A2 based on NMR longitudinal (T_1) relaxation measurements. *Arch. Biochem. Biophys. 384*, 47–58.
28. Zhang, Q., Ma, X., Ward, A., Hong, W., Jaakola, V., Stevens, R. C., Finn, M. G., and Chang, G. (2007) Designing facial amphiphiles for the stabilizaton of integral membrane proteins. *Angew. Chem., Int. Ed. 46*, 7023–7025.
29. Muralidhara, B. K., Negi, S., Chin, C. C., Braun, W., and Halpert, J. R. (2006) Conformational flexibility of mammalian cytochrome P450 2B4 in binding imidazole inhibitors with different ring chemistry and side chains. Solution thermodynamics and molecular modeling. *J. Biol. Chem. 281*, 8051–8061.
30. Davydov, D. R., Deprez, E., Hoa, G. H., Knyushko, T. V., Kuznetsova, G. P., Koen, Y. M., and Archakov, A. I. (1995) High-pressure-induced transitions in microsomal cytochrome P450 2B4 in solution: Evidence for conformational inhomogeneity in the oligomers. *Arch. Biochem. Biophys. 320*, 330–344.
31. Tsalkova, T. N., Davydova, N. Y., Halpert, J. R., and Davydov, D. R. (2007) Mechanism of interactions of α-naphthoflavone with cytochrome P450 3A4 explored with an engineered enzyme bearing a fluorescent probe. *Biochemistry 46*, 106–119.
32. Leslie, A. G. W. (1999) Integration of macromolecular diffraction data. *Acta Crystallogr. D55*, 1696–1702.
33. Kabsch, W. (1988) Evaluation of single-crystal X-ray diffraction data from a position-sensitive detector. *J. Appl. Crystallogr. 21*, 916–924.
34. McCoy, A. J., Grosse-Kunstleve, R. W., Adams, P. D., Winn, M. D., Storoni, L. C., and Read, R. J. (2007) Phaser crystallographic software. *J. Appl. Crystallogr. 40*, 658–674.
35. Murshudov, G. N., Vagin, A. A., and Dodson, E. J. (1997) Refinement of macromolecular structures by the maximum-likelihood method. *Acta Crystallogr. D53*, 240–255.
36. Emsley, P., Lohkamp, B., Scott, W., and Cowtan, K. (2010) Features and development of Coot. *Acta Crystallogr. D66*, 486–501.
37. Padilla, J., and Yeates, T. O. (2003) A statistic for local intensity differences: Robustness to anisotropy and pseudo-centerting and utility for detecting twinning. *Acta Crystallogr. D59*, 1124–1130.
38. Yeates, T. O. (1997) Detecting and overcoming crystal twinning. *Methods Enzymol. 276*, 344–358.
39. Kleywegt, G. J., and Jones, T. A. (1994) Detection, delineation, measurement and display of cavities in macromolecular structures. *Acta Crystallogr. D50*, 178–185.
40. Morris, G. M., Goodsell, D. S., Halliday, R. S., Huey, R., Hart, W. E., Belew, R. K., and Olson, A. J. (1998) Automated docking using a lamarckian genetic algorithm and empirical binding free energy function. *J. Comput. Chem. 19*, 1639–1662.
41. Helms, V., and Wade, R. C. (1995) Thermodynamics of water mediating protein-ligand interactions in cytochrome P450cam: A molecular dynamics study. *Biophys. J. 69*, 810–824.
42. Brunger, A. T., Adams, P. D., and Rice, L. M. (1997) New applications of simulated annealing in X-ray crystallography and solution NMR. *Structure 5*, 325–336.
43. Constantine, K. L. (2001) Evaluation of site-directed spin labeling for characterizing protein-ligand complexes using simulated restraints. *Biophys. J. 81*, 1275–1284.
44. Yue, S. Y. (1990) Distance-constrained molecular docking by simulated annealing. *Protein Eng. 4*, 177–184.
45. Eswar, N., Eramian, D., Webb, B., Shen, M. Y., and Sali, A. (2008) Protein structure modeling with MODELLER. *Methods Mol. Biol. 426*, 145–159.
46. DeLano, W. L. (2002) The PyMOL molecular graphics system, MacPyMOL ed., DeLano Scientific, Palo Alto, CA.
47. Van Der Spoel, D., Lindahl, E., Hess, B., Groenhof, G., Mark, A. E., and Berendsen, H. J. (2005) GROMACS: Fast, flexible, and free. *J. Comput. Chem. 26*, 1701–1718.
48. Oostenbrink, C., Soares, T. A., van der Vegt, N. F., and van Gunsteren, W. F. (2005) Validation of the 53A6 GROMOS force field. *Eur. Biophys. J. 34*, 273–284.
49. Darden, T., York, D., and Pederson, L. (1993) Particle mesh Ewald: An N-log(N) method for Ewald sums in large systems. *J. Chem. Phys. 98*, 10089–10092.
50. Hummel, M. A., Gannett, P. M., Aguilar, J. S., and Tracy, T. S. (2004) Effector-mediated alteration of substrate orientation in cytochrome P450 2C9. *Biochemistry 43*, 7207–7214.
51. Modi, S., Gilham, D. E., Sutcliffe, M. J., Lian, L.-Y., Primose, W. U., Wolf, C. R., and Roberts, G. C. K. (1997) 1-Methyl-4-phenyl-1,2,3,6-tetrahydropyridine as a substrate of cytochrome P450 2D6: Allosteric effects of NADPH-cytochrome P450 reductase. *Biochemistry 36*, 4461–4470.
52. Schoch, G. A., Attias, R., Belghazi, M., Dansette, P. M., and Werck-Reichhart, D. (2003) Engineering of a water-soluble plant cytochrome P450, CYP73A1, and NMR-based orientation of natural and alternate substrates in the active site. *Plant Physiol. 133*, 1198–1208.
53. Piotto, M., Saudek, V., and Sklenar, V. (1992) Gradient-tailored excitation for single-quantum NMR spectroscopy of aqueous solutions. *J. Biomol. NMR 2*, 661–665.
54. Prost, E., Sizun, P., Piotto, M., and Nuzillard, J. M. (2002) A simple scheme for the design of solvent-suppression pulses. *J. Magn. Reson. 159*, 76–81.
55. Modi, S., Paine, M. J., Sutcliffe, M. J., Lian, L.-Y., Primrose, W. U., Wolf, C. R., and Roberts, G. C. K. (1996) A model for human cytochrome P450 2D6 based on homology modeling and NMR studies of substrate binding. *Biochemistry 35*, 4540–4550.
56. Bruce, S. D., Higinbotham, J., Marshall, I., and Beswick, P. H. (2000) An analytical derivation of a popular approximation of the Voigt function for quantification of NMR spectra. *J. Magn. Reson. 142*, 57–63.
57. Marshall, I., Bruce, S. D., Higinbotham, J., MacLullich, A., Wardlaw, J. M., Ferguson, K. J., and Seckl, J. (2000) Choice of spectroscopic lineshape model affects metabolite peak areas and area ratios. *Magn. Reson. Med. 44*, 646–649.
58. Marshall, I., Higinbotham, J., Bruce, S., and Freise, A. (1997) Use of Voigt lineshape for quantification of in vivo ^{1}H spectra. *Magn. Reson. Med. 37*, 651–657.
59. Massiot, D., Fayon, F., Capron, M., King, I., Le Calvé, S., Alonso, B., Durand, J., Bujoli, B., Gan, Z., and Hoatson, G. (2002) Modelling

one- and two-dimensional solid-state NMR spectra. *Magn. Reson. Chem. 40*, 70–76.
60. Ammann, L. P., Merritt, M., Sagalowsky, A., and Nurenberg, P. (2006) Peak-finding partial least squares for the analysis of ^{1}H NMR spectra. *Chemom. Intell. Lab. Syst. 20*, 231–238.
61. Kuesel, A. C., Stoyanova, R., Aiken, N. R., Li, C. W., Szwergold, B. S., Shaller, C., and Brown, T. R. (1996) Quantitation of resonances in biological ^{31}P NMR spectra via principal component analysis: Potential and limitations. *NMR Biomed. 9*, 93–104.
62. Stoyanova, R., and Brown, T. R. (2001) NMR spectral quantitation by principal component analysis. *NMR Biomed. 14*, 271–277.
63. Kielkopf, J. F. (1973) New approximation to the Voigt function with applications to spectral-line profile analysis. *J. Opt. Soc. Am. 63*, 987–995.
64. Chen, H., Van Huffel, S., Van Ormondt, D., and De Beer, R. (1996) Parameter estimation with prior knowledge of known signal poles for the quantification of NMR spectroscopy data in the time domain. *J. Magn. Reson., Ser. A 119*, 225–234.
65. Viereck, N., Nørgaard, L., Bro, R., and Engelsen, S. B. (2006) Chemometric analysis of NMR data. In Modern magnetic resonance (Webb, G. A., Ed.) Springer, Dordrecht, The Netherlands.
66. Villafranca, J. J. (1989) Paramagnetic probes of macromolecules. *Methods Enzymol. 177*, 403–413.
67. Dwek, R. A. (1973) Nuclear magnetic resonance (N.M.R.) in biochemistry: Applications to enzyme systems, Oxford University Press, New York.
68. Davydov, D. R., Fernando, H., and Halpert, J. R. (2006) Variable path length and counter-flow continuous variation methods for the study of the formation of high-affinity complexes by absorbance spectroscopy. An application to the studies of substrate binding in cytochrome P450. *Biophys. Chem. 123*, 95–101.
69. Modi, S., Primrose, W. U., Boyle, J. M., Gibson, C. F., Lian, L. Y., and Roberts, G. C. (1995) NMR studies of substrate binding to cytochrome P450 BM3: Comparisons to cytochrome P450 cam. *Biochemistry 34*, 8982–8988.
70. Clore, G. M., and Iwahara, J. (2009) Theory, practice, and applications of paramagnetic relaxation enhancement for the characterization of transient low-population states of biological macromolecules and their complexes. *Chem. Rev. 109*, 4108–4139.
71. Iwahara, J., Schwieters, C. D., and Clore, G. M. (2004) Ensemble approach for NMR structure refinement against ^{1}H paramagnetic relaxation enhancement data arising from a flexible paramagnetic group attached to a macromolecule. *J. Am. Chem. Soc. 126*, 5879–5896.
72. Nishiya, Y., Hagihara, K., Ito, T., Tajima, M., Miura, S., Kurihara, A., Farid, N. A., and Ikeda, T. (2009) Mechanism-based inhibition of human cytochrome P450 2B6 by ticlopidine, clopidogrel, and the thiolactone metabolite of prasugrel. *Drug Metab. Dispos. 37*, 589–593.
73. Bauer, M., Bertario, A., Boccardi, G., Fontaine, X., Rao, R., and Verrier, D. (1998) Reproducibility of ^{1}H-NMR integrals: A collaborative study. *J. Pharm. Biomed. Anal. 17*, 419–425.
74. Shimizu, S., Atsumi, R., Nakazawa, T., Fujimaki, Y., Sudo, K., and Okazaki, O. (2009) Metabolism of ticlopidine in rats: Identification of the main biliary metabolite as a glutathione conjugate of ticlopidine S-oxide. *Drug Metab. Dispos. 37*, 1904–1915.
75. Yoneda, K., Iwamura, R., Kishi, H., Mizukami, Y., and Kobayashi, S. (2004) Identification of the active metabolote of ticlopidine from rat in vitro metabolites. *Br. J. Clin. Pharmacol. 142*, 551–557.
76. Yano, J. K., Denton, T. T., Cerny, M. A., Zhang, X., Johnson, E. F., and Cashman, J. R. (2006) Synthetic inhibitors of cytochrome P-450 2A6: Inhibitory activity, difference spectra, mechanism of inhibition, and protein cocrystallization. *J. Med. Chem. 49*, 6987–7001.
77. Yano, J. K., Hsu, M. H., Griffin, K. J., Stout, C. D., and Johnson, E. F. (2005) Structures of human microsomal cytochrome P450 2A6 complexed with coumarin and methoxsalen. *Nat. Struct. Mol. Biol. 12*, 822–823.
78. Caliandro, R., Carrozzini, B., Cascarano, G. L., De Caro, L., Giacovazzo, C., and Siliqi, D. (2008) The (*Fo*-*Fc*) fourier synthesis: A probabilistic study. *Acta Crystallogr. A64*, 519–528.